J Mater Sci: Mater Electron (2017) 28:8023–8028
DOI 10.1007/s10854-017-6507-4

Synthesis and luminescence properties of $NaLa(WO_4)_2$:Eu^{3+} phosphors for white LED applications

Anthuvan John Peter[1] · I. B. Shameem Banu[1]

Received: 8 November 2016 / Accepted: 30 January 2017 / Published online: 9 February 2017

Abstract Eu^{3+} activated $NaLa(WO_4)_2$ (NLW) red phosphors were synthesized via an ethylene glycol route at low temperature as 120 °C for solid state lighting applications. X-ray diffraction (XRD), field emission scanning electron microscope (FE-SEM), FT-IR, Raman, emission and excitation properties were studied for synthesized NLW phosphors. XRD analysis endorsed the formation of $NaLa(WO_4)_2$ with scheelite structure. For 9 mol% of Eu^{3+} concentration, the phosphor demonstrates an intensified narrow excitation peak at 394 nm indicating a strong absorption due to Eu^{3+} ion. The PL emission spectra of $NaLa(WO_4)_2$:0.09 Eu^{3+}phosphors exhibited an intense peak at 615 nm (red) which agrees to $^5D_0 \rightarrow {}^7F_2$ transition of Eu^{3+} at the excitation wavelength of 394 nm. The CIE colour coordinates of $NaLa(WO_4)_2$:0.09 Eu^{3+} red phosphor accord very well with the standard values of NTSC. The sterling luminescent properties of $NaLa(WO_4)_2$:0.09 Eu^{3+} phosphor executes it as a potential red phosphor upon near-UV LED excitation.

1 Introduction

The light emitting diodes (LEDs) have enticed great consideration as an illuminator for solid state lighting since 1993. Correlated with the conventional fluorescent lamps, solid state lighting technology has the benefits as low energy consumption, environmental stability and potent output and energy efficient [1–3]. The commercially gettable tricolor phosphors for White LEDs are Y_2O_2S:Eu^{3+} for red [4], $BaMgAl_{10}O_{17}$:Eu^{2+} for blue [5] and ZnS (Cu^+, Al^{3+}) for green [6]. While comparing with blue and green phosphors, the thermal and chemical stability of the sulphide based red phosphors are found to be inadequate. They exhibit poor absorbance in near UV region and their efficiency is also approximately eight times lesser than blue and green phosphors for white LED applications [7]. In order to get around this shortcoming, a well- efficient red-emitting phosphor to be synthesised is a vital part. Therefore, at the moment, significant attention is sharpened on finding an alternative novel low cost red phosphor which is thermally and chemically more stable and also exhibits more excellent luminous efficiency. Recently, a special class of Re^{3+} doped $NaLa(WO_4)_2$ tungstates are attractive and have been investigated intensely. The host (NLW) exhibits high chemical stability, very low phonon frequencies, optical transparency over a wide wavelength range and site-selective doping capability.Thus, It exhibits a wide range of applications in vivo imaging of tissues and cells, solid state light emitting applications, scintillators and thermally stimulated luminescence (TSL) dosimetry [8]. Among different rare earth elements trivalent europium (Eu^{3+}) ion is widely recognized as an activator for red emission (around 612 nm), which has been used in most commercial red phosphors. The intra-$_4$f-shell down-conversion transitions ($^5D_0$–^7F_j (j = 1, 2, 3, 4) of Eu^{3+} ions are strongly dependent on crystal structure of the host and sensitive to the local environment where the rare-earth has been situated [9]. Among all transition of Eu^{3+}, the transition due to $^5D_0$–$^7F_2$ is the most intense and hypersensitive transition and emits red color. The transition probabilities are strongly influenced by host lattice, specially the covalent nature of host and site symmetry of the occupation [10]. Also, most of the synthesis reports on these materials remain in the stage of solid phase

✉ Anthuvan John Peter
quantajohn@gmail.com

[1] Department of Physics, B. S. Abdur Rahman University, Chennai, India

synthesis or high temperature liquid techniques. These methods usually need high temperatures, time consuming heating processes and frequent grinding. The grinding process damages the phosphor surfaces, resulting in the loss of emission intensity. In addition, the aggregation and inhomogeneous shapes are also unavoidable, which inhibit the absorption of the excitation energy and therefore reduce the emission intensity [11, 12].

To the best of our knowledge, the reports focused on the synthesis and optical properties of rare-earth-doped $NaLa(WO_4)_2$ are still limited. Based on these investigations, in this paper, $NaLa(WO_4)_2:Eu^{3+}$ (x = 0.01, 0.05, 0.07, 0.09, 0.11) phosphors were at low temperature in ethylene glycol as reaction medium. The structural and optical properties of the materials were studied in detail.

2 Experimental

2.1 Synthesis

The phosphors of $NaLa(WO_4)_2:Eu^{3+}$ (x = 0.01, 0.05, 0.07, 0.09, 0.11) were synthesized at low temperature (140 °C reflexed for 2h) in ethylene glycol (EG) medium. Lanthanum(III) nitrate hexahydrate ($La(NO_3)_3{\cdot}6H_2O$, AR) Europium(III) oxide (Eu_2O_3, 99.99%, Aldrich), Sodium tungstate dehydrate ($Na_2WO_4{\cdot}2H_2O$, AR) were used as sources of La^{3+}, Eu^{3+} and WO_4^{2-} respectively. In a typical synthesis procedure, stoichiometric ratio of $La(NO_3)_3{\cdot}6H_2O$ and Eu_2O_3 were dissolved together in Conc. HNO_3 and excess acid was removed by evaporation with water. To this solution, stoichiometric ratio of $Na_2WO_4{\cdot}2H_2O$ was added followed by 50 ml of EG. The PH of the solution was balanced to have 9–9.5 using NaOH solution. The resulting solution was refluxed for 2 h at 140 °C. The resulting white precipitate was collected by centrifugation at 10,000 r min^{-1} for 15 min. The phosphor material is washed many times with acetone and finally dried under an ambient atmosphere. The dried sample was used for characterization.

2.2 Characterization

X-ray powder diffraction (XRD) analysis was out using Pan Analytical X'pert pro X-ray diffractometer with Cu K-alpha radiation (λ = 1.5406 Å) at a scanning rate of 0.020 per second. The XRD patterns were obtained in the range of $0° \leq 2\theta \leq 70°$ and were compared with the JCPDS data. Fourier Transform infrared spectroscopy (FTIR) measurements were carried out in the wavelength range of 400–4000 cm^{-1} with a Nicolet 6700 FTIR equipped with a deuterated triglycine sulfate detector. Raman spectra were recorded on a RFS/100/S Bruker FT-Raman spectrometer with a Nd doped yttrium aluminium garnet laser providing excitation light at 1064 nm in the frequency range of 150–1000 cm^{-1}. The size, shape and structure of the samples were characterized by emission scanning electron microscopy (FE-SEM, Hitachi S-$_4$800). Transmission electron microscopy (TEM) was recorded on a JEOL JEM-2100 at an accelerating voltage of 200 kV. The measurements of PL and excitation (PLE) spectra were performed by a Jobin Yuvon Flurolog-3-11 Spectroflurometer at room temperature with 450 W xenon lamp was used as the excitation source (200–700 nm). The excitation and emission slit width were set to 2 nm. All spectroscopic measurements of the phosphors were carried out at room temperature.

3 Results and discussion

3.1 Structural and morphology characterization

Figure 1 shows the XRD patterns of Eu^{3+} doped $NaLa(WO_4)_2$ phosphors with different doping concentration of Eu^{3+}. The diffraction patterns of $NaLa(WO_4)_2:xEu^{3+}$ fit well with the tetragonal scheelite crystal structure of $NaLa(WO_4)_2$ (JCPDS No. 79-1118). The strong and sharp diffraction peaks indicate a good crystallinity of the prepared samples. In addition, the diffraction intensities of all of the XRD patterns are sharp, revealing that the highly crystalline products can be synthesized by this method. The diffraction peaks of $NaLa(WO_4)_2:Eu^{3+}$ are shifted to higher angles when compared to that of standard $NaLa(WO_4)_2$ due to small ionic size of Eu^{3+} (106.6 pm) than La^{3+} (116.0 pm) and Na^+ (116.0 pm) in the host lattice. Lattice parameters were calculated for all NLW phosphors as shown

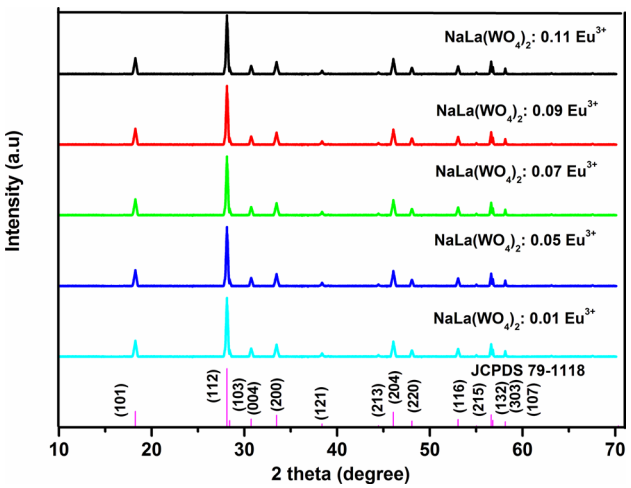

Fig. 1 XRD pattern of Na $La(WO_4)_2:xEu^{3+}$ (x = 0.01, 0.05, 0.07, 0.09 and 0.11)

Table 1 Lattice parameters of pure and Eu-doped NLW powders

Compound	*a* (Å)	*c* (Å)	Volume (Å^3)
Bulk crystal [14]	5.349	11.628	332.7
$NaLa(WO_4)_2$	5.3571 (1)	11.6625 (2)	336.13 (1)
$NaLa_{0,99}Eu_{0,01}(WO_4)_2$	5.3544 (4)	11.6612 (9)	335.65 (5)
$NaLa_{0,89}Eu_{0,11}(WO_4)_2$	5.3457 (4)	11.6443 (9)	335.48 (5)

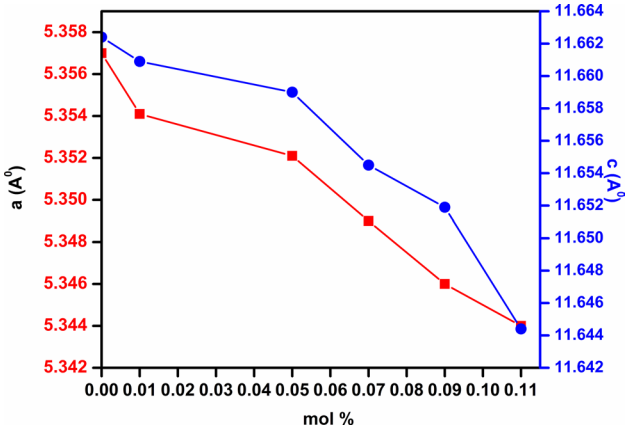

Fig. 2 Lattice parameters variations as a function of Eu concentration

in Table 1. The gradual decrease of the cell parameters due to the La substitution by Eu ions can be observed in Fig. 2. This result is justified since ionic radii of Eu^{3+} is smaller than of La^{3+} and Na^{+} for octahedral coordination [13] as in this case. The calculated values are comparable with those observed in bulk crystals [8]. Figure 3a shows the typical FE-SEM image of the as-prepared $NaLa(WO_4)_2$:0.09 Eu^{3+} phosphor. It can be found that the size and morphology of the product is not relatively uniform and regular. Meanwhile, some particles are agglomerated into bulk, which leads to the broad size range of particles. Figure 3b shows the TEM image of the as-prepared $NaLa(WO_4)_2$:0.09 Eu^{3+} phosphor. The products composed of a number of round nano-sized particles. The average grain size was estimated by counting 100 particles. Figure 3c show the statistic result of particle sizes. The average particle diameter of the as-prepared sample was estimated to be around 35 nm. The EDX spectrum of the sample prepared by this method confirms the presence of sodium (Na), Lanthanum (La), Tungsten (W) and oxygen (O) elements (Fig. 3d). No impurity peaks of other elements can be detected, which can effectively support the XRD result.

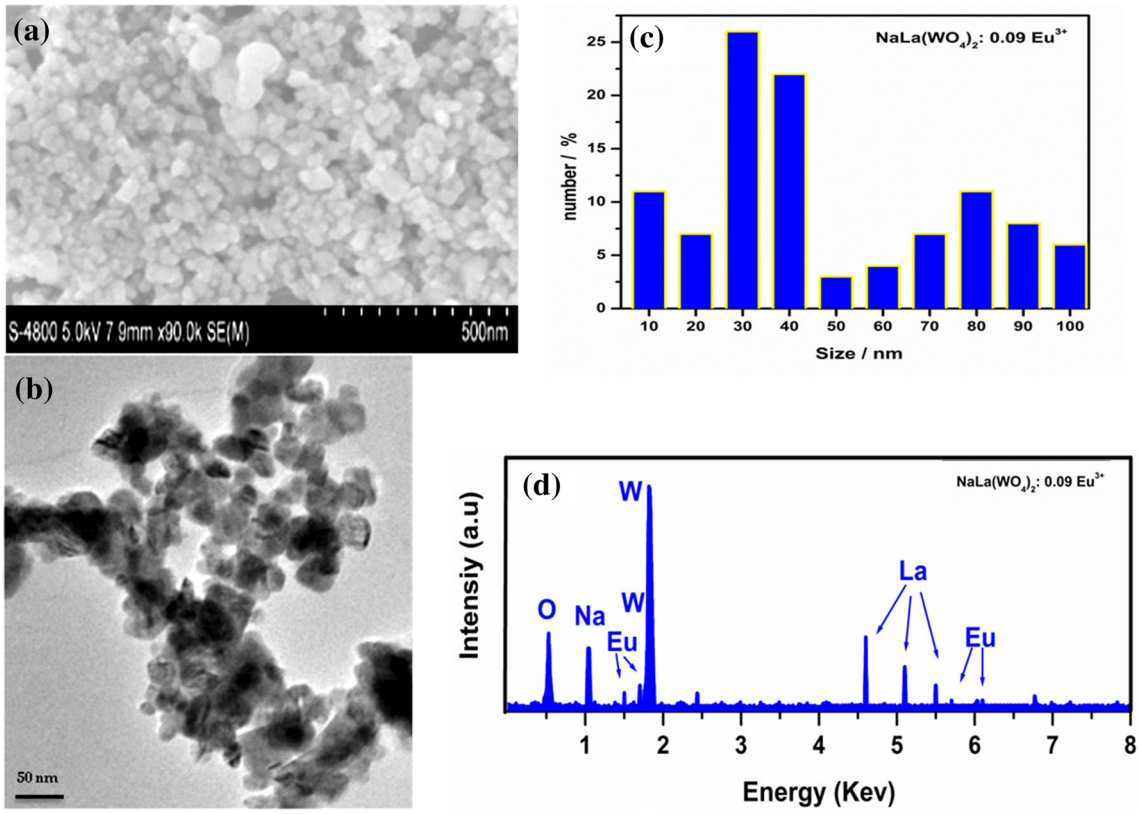

Fig. 3 **a** FE-SEM image of the as-prepared $NaLa(WO_4)_2$:0.09 Eu^{3+} phosphor. **b** TEM image of the as-prepared $NaLa(WO_4)_2$:0.09 Eu^{3+} phosphor. **c** Particle size analysis of the $NaLa(WO_4)_2$:0.09 Eu^{3+} phosphor. **d** EDX spectrum of $NaLa(WO_4)_2$:0.09 Eu^{3+} phosphor

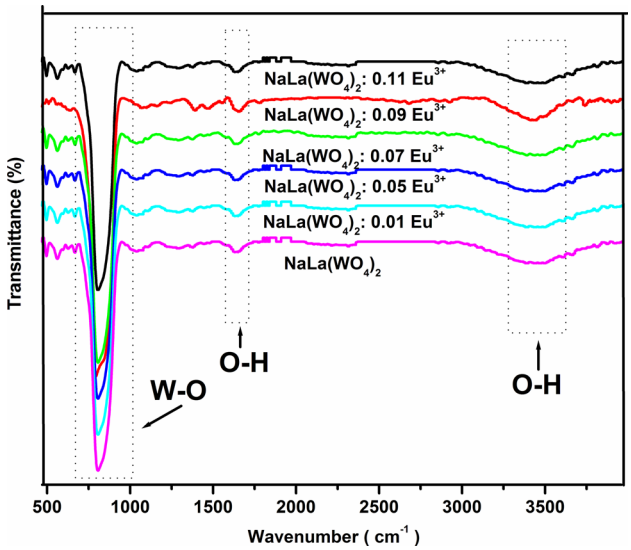

Fig. 4 Raman spectra of $NaLa(WO_4)_2$:xEu^{3+} (x = 0.01, 0.05, 0.07, 0.09, 0.11) phosphors

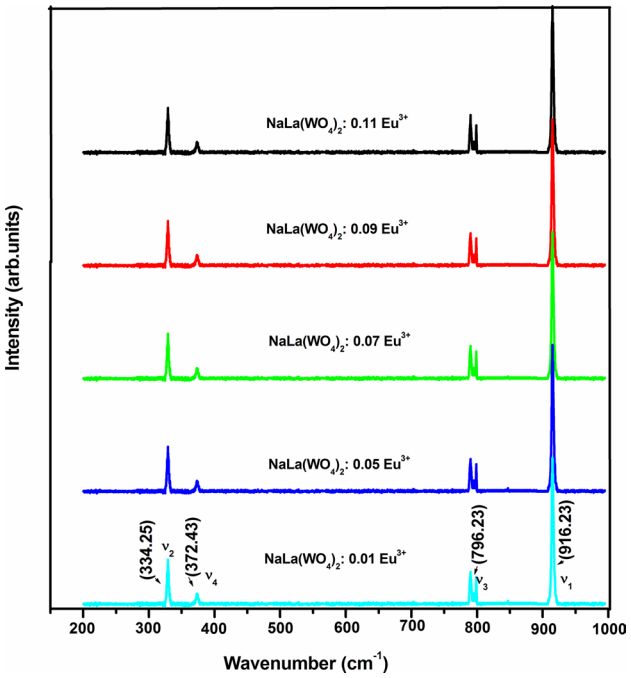

Fig. 5 FTIR spectra of $NaLa(WO_4)_2$:xEu^{3+} (x = 0.01, 0.05, 0.07, 0.09, 0.11) phosphors

3.2 FTIR analysis

The FT-IR spectra of the of $NaLa(WO_4)_2$:xEu^{3+} (x = 0.01, 0.05, 0.07, 0.09, 0.11) phosphors are shown in Fig. 4.The FTIR spectra show vibration bands due to the characteristic vibrations of W–O at around 1,000 cm^{-1}. The peaks at around 2960 cm^{-1} are due to stretching vibrations of CH_2 groups of EG molecule. A strong large absorption band around 657–966 cm^{-1} for $NaLa(WO_4)_2$:xEu^{3+} nano particles are related to anti-symmetric stretching vibration of O–W–O groups in WO_4^{2-} tetrahedron clusters. The bands at around 3419 and 1631 cm^{-1} can be referred to stretching vibration of O–H and H–O–H bending mode vibration of H_2O, respectively [14]. They are the usual vibrations of water molecules physically consumed on the sample surface from air, which is entirely different from coordinated water in compounds [15].

3.3 Raman analysis

The Raman spectra of $NaLa(WO_4)_2$:xEu^{3+} (x = 0.01, 0.05, 0.07, 0.09, 0.11) phosphors in the range from 200 to 1000 cm^{-1} is shown in Fig. 5. Raman spectra of the as prepared phosphor materials illustrates many peaks attributing to the Raman-active internal mode vibrations in the tetrahedral $[WO_4]^{2-}$ units. Those at around 916.23, 796.23, 372.43 and 334.25 cm^{-1} which correspond to $\nu 1(Ag)$,$\nu 3(Eg)$, $\nu_4(Bg)$ and $\nu_2(Ag)$ vibrations for $NaLa(WO_4)_2$ [17, 18]. The very small variations observed on the positions of Raman modes could be emerging from different influences, such as synthesizing methods, average crystal size and interaction forces between the ions [16]. An analysis of the spectra greatly exhibited that all Raman-active modes of $NaLa(WO_4)_2$:xEu^{3+} prepared in this work is component of a tetragonal structure and in agreement with those formerly reported in the literature [17, 18].

3.4 Photoluminescence properties, CIE chromaticity coordinates and thermal properties

Figure 6 shows the PLE spectra of the $NaLa(WO_4)_2$:xEu^{3+} (x = 0.01, 0.05, 0.07, 0.09 and 0.11) phosphor monitored at an emission wavelength of 615 nm. The PLE spectra of Na $La(WO_4)_2$:Eu^{3+} revealed a broad band between 220 and 300 nm with a band maximum at 249 nm, which is due to the charge transfer from the completely filled 2p orbital of O^{2-} ions to the partially filled 4f orbitals of Eu^{3+} ions [19, 20]. Thus, this band is also called as charge transfer band (CTB). The other excitation bands from 300 to 550 nm correspond to the intra configurational f–f transition of Eu^{3+} ions. The transitions were indexed as ($^7F_0 \rightarrow {}^5D_4$) at 361 nm, ($^7F_0 \rightarrow {}^5G_2$) at 381 nm, ($^7F_0 \rightarrow {}^5L_6$) at 394 nm, ($^7F_0 \rightarrow {}^5D_3$) at 412 nm, ($^7F_0 \rightarrow {}^5D_2$) at 462 nm, and ($^7F_0 \rightarrow {}^5D1$) at 530 nm. Figure 7 shows the PL spectra of the $NaLa(WO_4)_2$:xEu^{3+} samples with different Eu^{3+} ion concentrations monitored at an excitation wavelength of 394 nm. The PL spectra exhibited typical Eu^{3+} emission bands due to the presence of well known magnetic-dipole (MD) and electric dipole (ED) transitions. The photoluminescence emission spectra consists of sharp lines

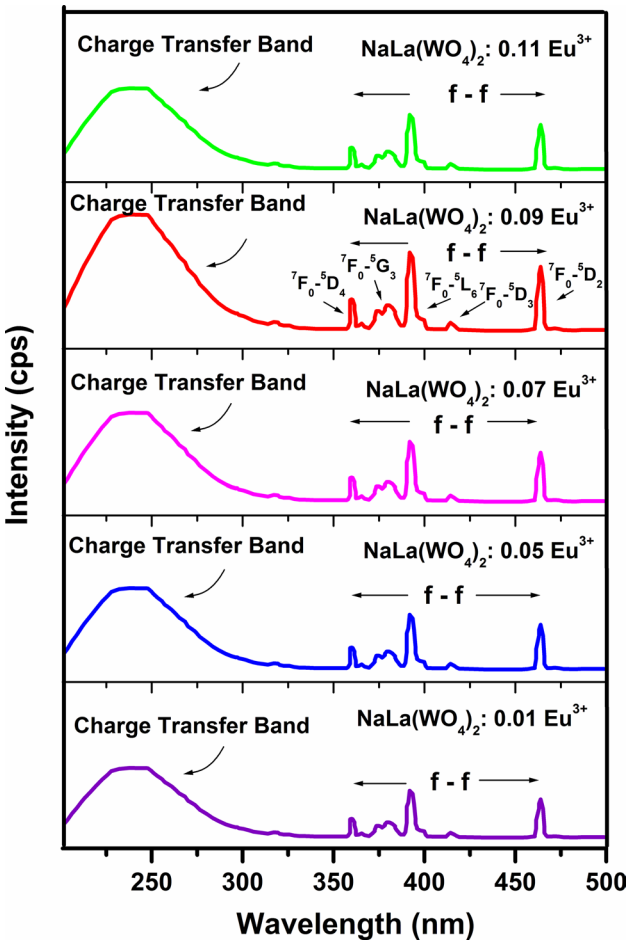

Fig. 6 PLE spectra of the $NaLa(WO_4)_2$:0.09Eu^{3+} monitored at an emission wavelength of 615 nm

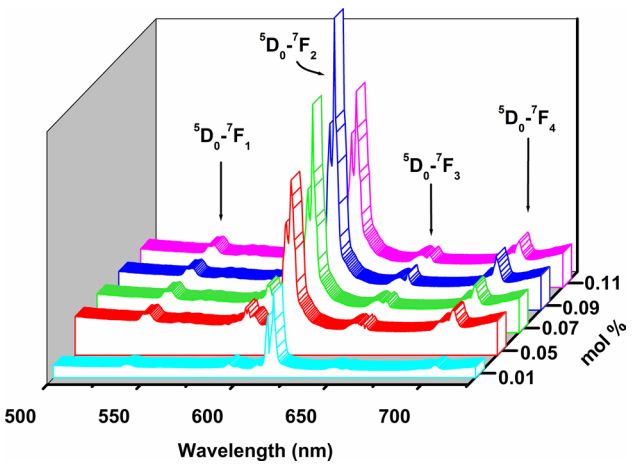

Fig. 7 PL spectra of the $NaLa(WO_4)_2$:xEu^{3+} (x = 0.01, 0.05, 0.07, 0.09 and 0.11) phosphors under the excitation wavelength of 396 nm

with wavelength ranging from 530 nm to 710 nm, which are associated with the $^5D_0 \rightarrow {}^7F_J$ (J = 1, 2, 3, 4) transitions from the excited Eu^{3+} to the ground state. The main emission peak is the $^5D_0 \rightarrow {}^7F_2$ transitions of Eu^{3+} at 615 nm; other transitions from $^5D_0 \rightarrow {}^7F_1$, $^5D_0 \rightarrow {}^7F_3$, and $^5D_0 \rightarrow {}^7F_4$ located in the range of 530–710 nm are weak [8]. The $^5D_0 \rightarrow {}^7F_2$ electric dipole transition of Eu^{3+} is highly sensitive to its surroundings and occurs dominantly only when the Eu^{3+} ion is in a noncentrosymmetric site. The emission intensity of the phosphor increases up to 9 mol% and then starts decreasing due to concentration quenching phenomena. As the Eu^{3+} ion concentration increased, the distance between Eu–Eu decreased and the energy was transferred non-radiatively between the Eu^{3+} ions, thus leads to the concentration quenching effect [21–25]. The lifetime of the Eu^{3+} ($^5D_0$–$^7F_2$) emission was measured and the normalized decay curves monitored for Na $La(WO_4)_2$:0.09 Eu^{3+} phosphors under excitation at 394 nm are shown in Fig. 8a. They fit well with the first-order exponential decay formula:

$$I(t) = Io^{+}A \exp(t/\tau) \quad (1)$$

where I and I_0 are the luminescence intensity at time t and 0, A is a constant, and τ represents the characteristic decay time for exponential component and the value of lifetime is 0.62 ms. The result shows that the lifetime is short enough for potential applications in displays and lights. The decay curve also indicates that all Eu^{3+} ions occupy the same atom environment, which is consistent with the description of the crystal structure above.

The thermal stability of the phosphor is an important area to be studied since the material is to be used in high-powered LEDs. The emission spectra measured for Na $La(WO_4)_2$:0.09 Eu^{3+} under 394 nm excitation at different temperatures between 25 and 250 °C are shown in Fig. 8b. The figure shows the temperature dependence of the luminescence quenching. The emission intensity of the phosphor decreases as the temperature increases up to 250 °C. Obviously, when the temperature increased to 150 °C, the corresponding PL intensity dropped to 81.3% of its initial value. This result indicates that the $NaLa(WO_4)_2$:0.09 Eu^{3+} phosphor has a relatively good thermal quenching effect. The thermal quenching phenomenon arises due to electron–phonon interaction and that can be very well explained using the configurational coordinate diagram. Initially, the Eu^{3+} luminescence center in the excited state is activated by phonon interactions which are released through a crossover between the $^5D_0$ excited state and ^7F_j (j = 1, 2, 3, 4) ground state [25, 26]. Thus, the emission intensity decreases as the temperature increases. CIE diagram (Fig. 8c) illustrates that the obtained phosphor nanoparticles show red emissions (x = 0.664, y = 0.336) when excited by a single wavelength (λ_{ex} = 394 nm) and

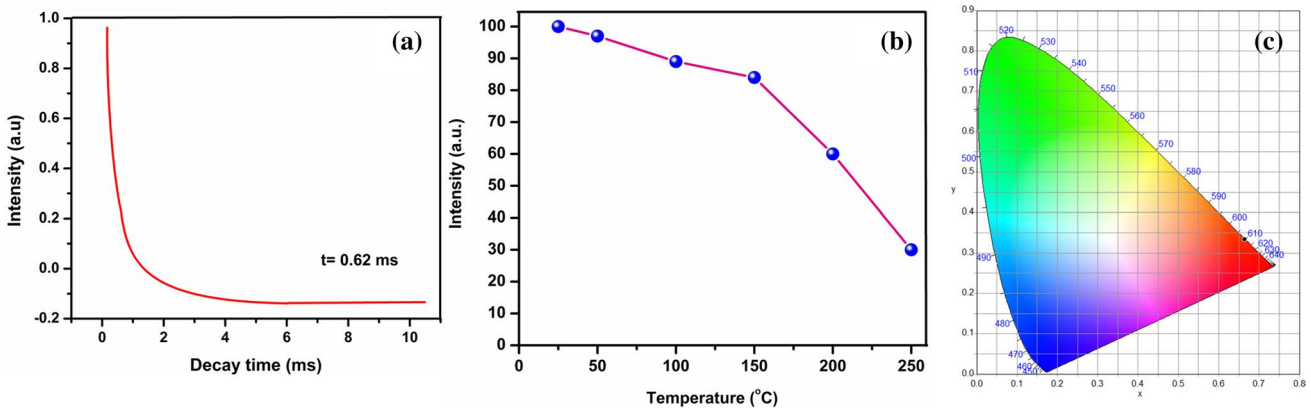

Fig. 8 **a** Representative emission decay curve for 615 nm ($^5D_0$–$^7F_2$ of Eu^{3+}) emission of 9 mol% Eu^{3+}-doped Na $La(WO_4)_2$ phosphor (λ_{exc} = 394 nm). **b** The PL spectra (λ_{ex} = 394 nm) of the $NaLa(WO_4)_2$:0.09 Eu^{3+} phosphor at different temperatures in the range of 25–250 °C. **c** CIE chromaticity diagram for $NaLa(WO_4)_2$:0.09 Eu^{3+} phosphor (λ_{ex} = 394 nm)

thus the obtained results confirm that the SSM prepared Na $La(WO_4)_2$:0.09 Eu^{3+} phosphor is a promising red emitting components for near-UV InGaN-based white LED.

4 Conclusion

Red emitting $NaLa(WO_4)_2$:xEu^{3+} phosphors have been successfully prepared at low temperature via ethyelene glycol route. Their structural and optical properties were discussed in detail. The XRD study reveals tetragonal structure for Eu^{3+} doped $NaLa(WO_4)_2$. Upon 394 nm near UV excitation, the $NaLa(WO_4)_2$:0.09Eu^{3+} phosphor showed strong red emission lines at 615 nm corresponding to forced electric dipole transitions. The optimum doping concentration of Eu^{3+} content in $NaLa(WO_4)_2$ for the red emission is found to be 9 mol%. All these favourable properties indicate that SSM prepared $NaLa(WO_4)_2$:0.09Eu^{3+} red phosphor is a promising candidate for the phosphor converted white LEDs.

References

1. C.H. Chiu, C.H. Liu, S.B. Huang, T.M. Chen, J. Electrochem Soc **155**, 3 (2008)
2. G. Du, W. Guo, J.M. Khalaf Al-zyadi, Y. Han, P. Liu, Z. Liu, J. Nanopart Res **15**, 5 (2013)
3. X. Lei, Z. Li, Y. Du, D. He, Y. Wang, L. Li, H. Jiao, J Mater Sci **48**, 14 (2013)
4. J. Dhanaraj, R. Jagannathan, D.C. Trivedi, J Mater Chem **13**, 7 (2003)
5. H.K. Jung, D.W. Lee, K.Y. Jung, J.H. Boo, J. Alloys Compd. **390**, 1–2 (2005)
6. Y.Y. Chen, J.G. Duh, B.S. Chiou, C.G. Peng, ,Thin Solid Films **392**, 1 (2001)
7. M. Thomas, P. Prabhakar Rao, M. Deepa, M.R. Chandran, P. Koshy, J. Solid StateChem **182**, 1 (2009)
8. L.L. Li, L. Liu, W.W. Zi, H. Yu, S.C. Gan, G.J. Ji, H.F. Zou, X.C. Xu, J Lumin **143**, 14–20 (2013)
9. I.L.V. Rosa, A.P.A. Marques, M.T.S. Tanaka, D.M.A. Melo, E.R. Leite, E. Longo, J.A. Varela, J Fluoresce **18**, 2 (2008)
10. J. Thirumalai, R. Krishnan, I.B. Shameem Banu, R. Chandramohan, J. Mater. Sci. **24**, 253 (2013)
11. Y. Yang, X. Li, W. Feng, W. Yang, W. Li, C. Tao, J. Alloys. Compd. 509, 3 (2011)
12. Y. Jin, J. Zhang, S. Lu, H. Zhao, X. Zhang, X.J. Wang, J. Phys. Chem. C **112**, 15 (2008)
13. D. Lide, *The CRC Hand book of Chemistry and Physics on CD-ROM, Version 2002*, (CRC Press, Boca Raton, 2002), pp. 12–13
14. A.P.A. Marques, M.T.S. Tanaka, E. Long, E.R. Leite, I.L.V. Rosa, J Fluoresc **21**, 3 (2011)
15. G. Li, Z. Wang, Z. Quan, C. Li, J. Lin, J. Crystal Growth Des **7**, 9 (2007)
16. N. Du, H. Zhang, X.Y. Ma, D.S. Li, D.R. Yang, Mater. Lett **63**, 1180 (2009)
17. A.B. Campos, A.Z. Simoes, E. Longo, J.A. Varela, V.M. Longo, A.T. de Figueiredo, F.S. de Vicente, A.C. Hernandes, Appl. Phys. Lett. **91**, 051923 (2007)
18. S.P.S. Porto, J.F. Scott, Phys. Rev **157**(3), 716–719 (1967)
19. V. Sivakumar, U.V. Varadaraju, J Electrochem. Soc. **152**, 10 (2005)
20. X.X. Wang, J. Wang, J.X. Shi, Q. Su, M.L. Gong, Mater. Res. Bull. **42**, 9 (2007)
21. F.N. Shi, J. Meng, Y.F. Ren, J Solid State Chem. 121, 1(1996)
22. X.H. He, M.Y. Guan, J.H. Sun, N. Lian, T.M. Shang, J. Mater. Sci. **45**, 1 (2010)
23. A. Xie, X. Yuan, F. Wang, Y. Shi, Z. Mu, J. Appl. Phys. D 43,5 (2010)
24. J. Wang, X. Jing, C. Yan, J. Lin, J. Electrochem. Soc. **152**, 3 (2005)
25. G.Y. Lee, J.Y. Han, W.B. Im, S.H. Cheong, D.Y. Jeon, Inorg. Chem. **51**, 10688 (2012)
26. W. Kemp, *Organic Spectroscopy*, 3rd edn. (Macmillan Hampshire, Basingtoke, 1975), p. 72